Articles in PresS. Am J Physiol Heart Circ Physiol (October 19, 2012). doi:10.1152/ajpheart.00499.2012

The Scanning Ion Conductance Microscope (SICM) for Cellular Physiology

Max J Lab, Anamika Bhargava, Peter T Wright and Julia Gorelik*

Imperial College London, National Heart & Lung Institute,
Imperial Centre for Experimental and Translational Medicine,
Hammersmith Campus,
Du Cane Road,
London W12 0NN, UK.

Running Head: SICM for Cellular Physiology

***Corresponding author**

Dr. Julia Gorelik
Imperial College London
National Heart and Lung Institute
4th floor, Imperial Centre for Translational and Experimental Medicine
Hammersmith Campus
Du Cane Road
London W12 0NN, UK
Tel 44(0)2075942736
Fax 44 020 7594 3653
E-mail: j.gorelik@imperial.ac.uk

Abstract

The quest for non-optical imaging methods that can surmount light diffraction limits resulted in the development of Scanning probe microscopes, however most of existing methods are not quite suitable for studying biological samples. The scanning ion conductance microscope (SICM) bridges the gap between the resolution capabilities of atomic force microscope and scanning electron microscope and functional capabilities of conventional light microscope. A nanopipette mounted on a three-axis piezo-actuator, scans a sample of interest and ion current is measured between the pipette tip and the sample. The feedback control system always keeps a certain distance between the sample and the pipette so the pipette never touches the sample. At the same time pipette movement is recorded and this generates a 3D topographical image of the sample surface. SICM represents an alternative to conventional high-resolution microscopy, especially in imaging topography of live biological samples. In addition the nanopipette probe provides a host of added modalities, for example using the same pipette and feedback control for efficient approach and seal with the cell membrane for ion channel recording. SICM can be combined in one instrument with optical and fluorescent methods and allows drawing structure-function correlations. It can also be used for precise mechanical force measurements as well as vehicle to apply pressure with precision. This can be done on living cells and tissues for prolonged periods of time without them loosing viability. The SICM is a multifunctional instrument, and it is maturing rapidly and will open even more possibilities in the near future.

Keywords:

Cardiomyocytes, Cell mechanics, FRET, Smart patch-clamp, Topography, SICM

Introduction

The resolution of conventional microscopy has light diffraction limits (Table 1). Electron microscopy surmounts this wavelength limit (15, 78), as does the non-optical Scanning Probe Microscope (SPM). It does this by using nanoprobes (20, 46, 52, 83, 92, 115). The probe, mounted on a three-axis actuator platform scans a sample of interest in the X and Y dimensions and together with recording of displacement in the Z dimension generates a 3D image. Binnig and Rohrer scanned the first samples using the Scanning Tunnelling Microscope (STM) in 1982, for which they received the Nobel Prize. Electrons 'tunnel' between the surface of interest and a very sharp stylus formed by a single atom enabling the mapping of surface topography. Placing biological samples on a conductive base, the STM went on to image their surfaces at very high resolutions (3). More recently, the self-assembly of subunits of proteins (amino acids and peptides) was studied using STM (121). The STM was the predecessor of other Surface Probe Microscopes, including the prevalent atomic force microscope (AFM) (7) (Table 1). The AFM uses a sharp tip mounted on a flexible cantilever, and the tip-sample interactions during scanning deflect the tip which produces very high resolution images. This technology has developed over time (1) and using an oscillating cantilever tip, has imaged large molecules (94) including DNA (9). Due to the ability of AFM to image non conducting surfaces, it has been widely used in biology to study cellular macromolecules like protein-nucleic acid complexes, chromosomes, cellular membranes and microbes. Recently, it has also been used for determining the mechanical properties of skinned myocardial cells (126). The technique of nanoindentation, traditionally performed via dedicated indenters can now be reliably achieved using AFM instrumentation, enabling mechanical property determination at the nanoscale. AFM nanoindentation capabilities have provided an

excellent improvement over conventional nanomechanical tools and by integration of topographical data from imaging, enabled the rapid extraction and presentation of mechanical data for biological samples (1). For example Jacot et al (50) measured the elastic modulus of the epicardium using atomic force microscope indentation and found that it significantly changes at birth, from an embryonic value of 12+/-4kPa to a neonatal value of 39+/-7kPa. This change is in the range shown to significantly affect the development of neonatal cardiomyocytes.

Biological cell surfaces commonly have a complex 3D nano-structure associated with complex and dynamic function. The AFM's intermittent contact imaging mode or 'tapping mode' circumvents these problems somewhat, and has been used for imaging of biological cells and molecules (2, 13, 14, 27, 71, 87, 95, 108).

However, the use of force in AFM can be problematic in studying biological samples. The cantilever tips can distort the image (123). Consequently this is an invasive technique albeit at the nanometre scale. However, reducing the force reduces surface indentation and improves its resolution, to reveal complex subcellular structures such as microvilli (69). The other major method of probing biological surfaces is scanning electron microscope (SEM), but it can only indirectly study remnants of cell behaviour after the cells have been fixed (frozen) (41, 76).

By contrast, optical methods, and in particular fluorescent microscopy, are more suited to study functionality by localizing fluorescently labelled molecules within the cell. But this does not directly image cell surfaces (74, 119), neither can it reach the resolution of the above two methods (Table 1). However, the Scanning Ion Conductance Microscope (SICM) bridges the gap between the resolution capabilities of AFM / SEM, and functional capabilities of conventional light microscopy (Table 1).

1. Principle of SICM Operation

Scanning Ion Conductance Microscopy is a relatively new technique, first used by Paul Hansma in 1989 (40). Its development was continued by Yuri Korchev starting in 1997 (35, 55, 57-61). In this microscope a sharp borosilicate glass nanopipette (with the inner diameter below 200 nm) is used as a probe.

The pipette can move during the scan, or as in Figure 1, the sample moves, being similarly mounted on the XY piezo. In this case, the pipette does not move laterally, just vertically (Z). To start, the pipette approaches the sample progressively decreasing the pipette-sample distance. This gradually restricts ions flowing through the fluid-filled pipette thus decreasing the current. The ion current through the pipette depends on the overall resistance of the tip, which is the combination of the resistance of the micropipette itself and the access resistance of the micropipette opening. Access resistance is a complex function of the distance between the sample and the probe, and the geometry and electrochemical properties of the sample surface. This current (I) through the pipette, which is measured directly, is given by:

$$I = V/Rp + Ra(d)$$

Where V = voltage applied to the electrode, Rp = pipette resistance, Ra = access resistance and d = distance between sample and the probe.

A distance-modulated feedback control system keeps the ionic conductance and thus the sample/pipette distance constant. Typically the feedback control stops the approach at a pre-defined distance or "set point". With the feedback loop controlling ion conductance the pipette never touches the sample – it stops at a distance equivalent to the inner radius of the pipette. This enables non-contact scanning. As the scan proceeds in the X and Y directions the ion conductance control system

detects changes in nanopipette displacement in the Z direction. These recorded signals build up a computerised 3D image of the sample surface (Figure 1).

The pipette's inner tip diameter is typically 20-100 nm. As the resolution depends upon the radius of the pipette inner tip (97), the SICM can obtain a resolution of 10 nm with a tip size of 20 nm diameter. The limitation of the tip size is around 10-12 nm.

In order to scan living cells, we require displacements in excess of 50 μm. Therefore, the SICM uses a 3 axis piezo translation stage (Jena, Germany) with 100 um travel distance in X Y and Z directions. This can image an area of 100 x 100 μm in a single scan. The lateral image resolution is usually 512x 512 pixels. A single scan can take several minutes depending on the resolution at which it is being acquired, and the area scanned. For example a 10 x 10 μm scan of an isolated adult cardiomyocyte with 150 nm resolution takes between 2-3 minutes. Although the SICM's resolution is not as high as that of the AFM, SICM is potentially an alternative to conventional high-resolution microscopy technologies, especially in the imaging of live biological samples (e.g. Figure 2). Importantly, the pipette probe provides a remarkable set of added capabilities (55, 107, 112). As described below, this multi-functionality makes the SICM a platform for the convergence of different microscopic and investigative technologies.

2. Typical hardware of SICM

A typical SICM uses an inverted microscope (e.g. Diaphot 200 or TE200; Nikon Corporation, Tokyo, Japan). Sample positioning is achieved by a computer-controlled piezotranslation stage mounted on the microscope stage (ICnano sample scan system -Ionscope Ltd, UK) with 100 x 100 μm x–y piezo-actuator for sample movement and a 25 μm z-axis piezo-actuator for pipette movement. The piezo

stage holds the glass nanopipette, which is connected to the head-stage of the feedback amplifier (Figure 1).

The SICM can use either a resistive or capacitive feedback head-stage like Axopatch 200B or Multiclamp 700B (Molecular devices Sunnyvale, CA). Ag/AgCl electrodes, in the bath and pipette, provide electrical connection as in a conventional electrophysiological circuit. Additional electronic components include a digitizer and computer controlled software. The SICM has stringent requirements to cope with vibration and electrical noise - particularly for "smart patch-clamp." The SICM setup rests on a vibration isolation table commonly used in electrophysiology. A small faraday cage on the microscope stage encloses the piezo axis translation stage, for electrical isolation and minimising noise.

3. "Hopping Probe" Scanning Ion Conductance Microscope (HPSICM)

Tall structures on the surface of biological cells can pose problems in lateral scanning. The pipette tip may collide with and drag the structures producing image artefacts, or the tip can break. To overcome this, Pavel Novak and colleagues developed the "hopping" mode of the SICM (HPSICM) as a modification of the scanning procedure (86). In a system with this modification, the pipette "hops" as it scans and it no longer needs continuous feedback to keep a fixed sample-probe distance. The pipette starts well above a surface feature, producing a maximal current at this starting distance from the surface. From this point the pipette approaches, reducing the ion current to a pre-defined 0.25-1%. The height of the sample at this imaging point is the recorded Z-position. With the ion current reduced by 1%, the tip is still at a one inner pipette radius from the surface and still avoids cell surface contact. The pipette withdraws and then the sample moves laterally to the next imaging point. Importantly, by updating the maximal current continuously while the pipette is withdrawn from the surface, the system

automatically compensates for slow drift in pipette current. HPSICM also minimises image-distorting noise as the pipette spends most of its time away from the image sampling point of interest. A direct comparison between images of soft biological samples obtained with the AFM and SICM showed that the SICM images were better than AFM which distorts the image (96).

4. Imaging of cell surface topography.

The SICM has produced 3D topographical images of cells that are unfixed, unstained, and alive, with resolutions approaching that of AFM and electron microscopes (96, 106). For SICM imaging, living cell samples need no fixing or mounting. Cells are placed in petridishes or on the coverslips on which they were grown. In the latter case, for purely topographical studies the cells are bathed in growth media, which is also used to fill the pipette. In other studies, for example "smart" patch-clamp, the external (bath solution) and internal (pipette solution) are determined by the requirements of the electrophysiological study (e.g. ion channel studies (35)).

Images of mouse ear hair cells were produced using SICM which have a true fidelity, as demonstrated when comparing them with images produced with a scanning electron microscope after cells were fixed and shaded. Surface topographical images of cardiomyocytes show complex structures with grooves related to the Z disc, with invaginations that represent T-tubule openings (Figure 2A & C). One can calculate the average length of Z-grooves on the surface of the myocytes to produce a measurement of the surface structure regularity. This indicator has proven to be valuable in following surface structural changes in cardiomyocytes that occur during heart failure (72). SICM cardiovascular imaging has not been confined to myocardial cells and for example images of aortic and heart valve endothelium have been obtained. Endothelial cells from aorta were

cultured in transwell plates under static conditions or on an orbital shaker that generated shear stress. In static conditions endothelial cells oriented randomly but when shear stress was applied they became aligned (93). In another study the fragments of living aortic tissues were examined. Endothelium from the outer curve of aorta showed orientation along the direction of blood flow, whereas the inner curve showed no orientation. This has been demonstrated in the past with other microscopy techniques but SICM resolves this physical alignment in living tissue. Also SICM has been applied to study the differences between membrane compliance in these cells (93).

5. Structure-Function Correlation.

Compartmentalization of calcium (5, 43, 89) and other second messengers (12, 47, 63) is crucial to cellular function. The plasma membrane is rich in receptors and ion channels that respond to corresponding ligands by generating second messengers in signaling microdomains. For example G-Protein Coupled Receptors can change their signaling properties depending on their cellular locations (11, 120). Protein kinases and phosphatases can also form structurally determined microdomains by specific localization to the cytoskeleton thus facilitating heterogeneous compartmentation (102). The AFM has been used to localize membrane receptors in cardiac tissue by combining fluorescence imaging and topography (23), but the SICM expands this type of use, which we will describe in the following section.

6.1. Localized beta adrenergic receptor-dependent cAMP signaling.

Combining SICM with Foster Resonance Energy Transfer (FRET) technique allowed Nikolaev et al to follow nano-scale signaling changes in defined sub-cellular regions, in living cardiomyocytes (Figure 2) (85). The SICM resolved T-tubules openings on the membrane of cardiomyocytes (Figure 2C) expressing a FRET sensor (EPAC2-camps) for the second messenger cAMP. When selectively stimulating beta-2

receptors (β_2AR), cAMP was only produced when applying its agonist selectively above a T-tubule, and the resultant cAMP signal was spatially confined (Figure 2D). This provides a degree of control for the β_2AR signaling mechanism - A situation in contrast to the beta-1 receptor (β_1AR) signaling, which is not spatially confined and is present equally in all membrane regions. In failing cardiomyocytes (Figure 2E), β_2AR signal was no longer constrained to the T-tubules (Figure 2F), which may be a contributory factor in the pathology of heart failure. They redistributed from the T tubules to the crests. This alters cyclic-AMP signal compartments with possible pathophysiological consequences.

This hybrid SICM/FRET technique may be an important avenue in studying other localized receptors. Moreover, as well as responses to pharmacological stimuli, SICM/FRET could investigate molecular mechanosensitivity. Recent studies by the Schwartz group (33) used a FRET sensor based on vinculin to resolve piconewton stresses on vinculin in focal adhesions. We could envisage a possible future development of SICM/FRET in this direction. By applying pressure via the SICM pipette a combination of SICM and a FRET sensor could investigate these dynamic processes. It could also investigate cellular networks and contacts to monitor the effects of stimulating single cells in a network, of adherent cells.

6.2 Mapping ion channels with an added patch system.

The SICM has been combined with a conventional whole-cell patch-clamp setup. In this combination, the SICM non-contact scan can provide a map of the location of KATP channels (60). In this setup current images were recorded over some 40 min and showed low lateral mobility of KATP channels, but they concentrate in sarcolemmal *Z* grooves. The SICM pipette with K^+ inside, applied K^+ while scanning the cell surface. A second patch-clamp pipette in the whole-cell mode records patch currents as the SICM probe scans over and activates a KATP channel. This

information can be related to the position of the SICM probe to create a distribution map of KATP channels, or with appropriate activation and markers, other particular ion channels.

6.3 Mapping Ion Channels with SICM as the Patch-Clamp System (The "Smart Patch-Clamp" technique)

The mapping of ion channels has been facilitated by using the same pipette both to image the surface of a cardiomyocyte and to function as the electrophysiological probe. In this technique, a high resistance glass nanopipette first scans the cell surface to produce a high-resolution topographic image of the cell surface. The topographic image is used to precisely position the pipette onto a cellular nanodomain of choice (we have the XY coordinates.) The same glass nanopipette is then used to obtain single ion channel currents using the patch-clamp technique. In the conventional patch-clamp technique the pipette approaches the target manually and often obliquely to visualise the pipette tip placement through the microscope. By contrast, pipette-approach with the SICM is vertical, almost fully automatic, and precisely controlled by the distance modulated feedback system. At a predetermined distance from the precisely selected target location the feedback control is switched off to allow a controlled contact with the membrane. The frequency of successful patches is significantly higher with this approach than with the conventional method (31). SICM distance-modulated feedback control is useful as the glass pipette will not touch the cell until required, and damage to the cell or pipette is minimised. As a result, "smart" patch-clamp technique records ion channel activity from precise nanodomains on the surface of live cells and thus can generate a spatial functional map of surface ion channels. This is in contrast to conventional patch-clamping where the position of the pipette with respect to the cell topography cannot be controlled with a nanoscale precision. The method is also

superior to the current conventional microscopic techniques (immunofluorescence) which target all the channels including the dormant ones, whereas the "smart" patch-clamp technique locates only the functional ion channels.

Yuri Korchev and co-workers developed and successfully applied the "smart" patch-clamp to record ion channels from several different cell types (31, 35). Ion currents were recorded from very small cells (e.g. sea urchin sperm cells) and fine focal swellings (boutons) in neuronal processes of 0.5-1.0 μm in diameter, which otherwise would have been extremely difficult to patch. That is, it can successfully record from membrane structures that are too small to be resolved conventionally or that cannot be detected by light microscopy e.g. from T-tubules of cardiomyocytes. The "Smart" patch-clamp system produced a spatial map of L-type calcium channels on a cardiomyocyte surface (setup shown in Figure 3B). Figure 3A shows the optical image of an isolated cardiomyocyte and position of the nanopipette. Figure 3C shows a 10 μm x 10 um topography scan of the same cardiomyocyte. "Smart" patch-clamp at different locations (e.g. T-tubules, crest or groove, Figure 3D) provided the first direct evidence of functional ion channel location. A representative L-type calcium channel activity from a T-tubule is shown in Figure 3E. The study showed a preferential location of L-type calcium channels to the T-tubules (Figure 3F) where they are in close proximity to other proteins involved in excitation-contraction coupling (6, 88).

The "Smart" patch-clamp also recorded ion channel currents from opaque samples (e.g. aorta, brain slices, and cells grown on filters). Optically guided patch-clamp prevents the collection of any information on the position or type of cellular structure. In another study, Gu and co-workers mapped not only calcium channels but also chloride channels on the surface of cardiomyocytes and found that these are not randomly distributed but have a specific location on cardiomyocyte

membrane (three Cl− channels are located only in *z* grooves and T-tubule openings) where they may have synergistic roles in excitation-contraction coupling (35).

A. K. Dutta and co-workers used smart-patch to record maxi-anion channels from cardiomyocytes which could not be recorded using conventional patch-clamp (24). The advantage of "smart" patch-clamp here would be to visualize structures where the ion channels could be clustered which could easily be missed in conventional patch-clamp.

6. Tracking Dynamic Biological Processes

7.1 Dynamics of membrane structures.

Unlike the other high resolution microscopes, the fact that the SICM can scan live cells in real time means it can follow biological processes taking place at cell membrane surfaces (125) including large membrane proteins (104, 106). In the high resolution mode the SICM can scan an area of 1 μm square in 9 seconds per frame. This can follow the appearance and disappearance of microvilli and the opening and closing of endocytotic pits. With the improved topographical resolution, Shevchuk et al (105) found that the SICM can visualize the opening and closing of clathrin pits, which are ~200-nm indentations in the membrane. It appears that most pits close with the help of a membrane protrusion that forms beside the pit. After simultaneous confocal detection of fluorescence in cells expressing GFP-labelled proteins they found that clathrin, dynamin and several other actin-binding proteins, for example Flotillin 1 and 2 co-localize with pits when these undergo morphological changes.

The SICM has revealed movements and reorganization of microvilli in real time on the surface of different types of epithelial cells (32). Microvilli appear and grow at a rate of about 5 nm/s over 2 and a half minutes, and after reaching a plateau lasting

some 5 minutes and retract at about 1.2 nm/s. Moreover, they tend to form migrating clusters.

7.2 Cell Volume Measurements

Cell volumes can dynamically change. Osmotic changes following early myocardial ischemia and cell changes in myocardial hypertrophy require complex cell-shape and volume reorganization (38, 45). Several indirect techniques (16, 53) and some more direct methods(84) have been used to measure and monitor cell volume. The latter method is only applicable to cells of nearly spherical shape and in suspension. Light microscopy methods have also been used (26, 75). An advanced method for cell volume measurement uses scanning laser confocal microscopy (25, 36, 127). However, generally, these methods have limited spatial resolution, and the cell plasma membrane cannot always be clearly visualized. The SICM can measure cell volumes between 10^{-19} and 10^{-9} litre (58) The SICM measures volume by integrating the raster image (Z-displacement) in X and Y directions, of the whole cell assuming that the entire cell's basal surface is in close contact with the substrate (58). As a reference, we measure the Z position of the pipette touching the substrate. This technique can also measure smaller volumes such as in lamelopodia, dendritic processes, or microvilli, with 2.5 x 10^{-20} liter resolution.

7. SICM as a Non-Invasive Mechanical (Distance and Force) Probe

8.1 Contraction

Hovering over a contracting myocyte the SICM distance feedback control can follow and record Z-displacement of the nanopipette and therefore record the event of contraction as an upwards membrane movement. Figure 4A diagrams the system for recording contraction and monitoring calcium transients. The system records and digitizes the Z piezo position which follows the physical contraction of the membrane (Figure 4B – black trace)

8.2 Cell membrane compliance

Cellular mechanical properties are determined by its intracellular mechanical characteristics such as cell structures, molecules, and downstream signals associated with the cytoskeleton (51). On the other hand, mechanical properties of the cell membrane contribute to cellular function (90). Being heterogeneously supported by the cytoskeleton, membrane varies its mechanical properties at the nanoscale. It is important to use adequate mechanical investigative tools while studying cells that are alive and with soft surfaces.

Different methods have been applied to study membrane compliance, e.g. micropipette aspiration (44) and optical tweezers (17, 111). The AFM's cantilever can measure forces at the molecular level (73, 113, 114, 124), and it has also proved to be suitable for mapping local mechanical properties at nano-scales (21, 22, 37, 42, 68, 99, 103, 109) and relate this to cell topography. It has shown heterogeneity of micromechanical properties of cultured atrial myocytes, which correlated with cytoskeletal structure (fluorescence imaging). Pressing the AFM's cantilever on to cell surfaces has studied cell compliance and elasticity (2, 28, 64, 117).

But as described above, the AFM's cantilever directly and undesirably contacts the cell surface. Any use of force in these soft cell membranes will compromise attempts at determining any heterogeneity in the cell's mechanical properties. The SICM based system overcomes some of these difficulties (100), and its distance control may be employed to probe cell mechanics. A pressure source down the nanopipette generates force at the tip. This force is calibrated, using the AFM cantilever as the gold standard, with applied pipette pressure bending the cantilever. The SICM distance feedback control ensures the pipette follows the

bending lever. Pipette pressure is converted to force (100) and the pressure applied at the pressure port is developed at the pipette tip.

Using hydraulic jets applied to indent surface membranes, the SICM has studied the mechanical properties of some cell types (100).

We (100) initially calibrated the SICM using an AFM cantilever with a spring constant of 0.01 N/m. Pipette pressure on the cantilever bends the lever, and we can measure the corresponding change in pipette position. Control experiments over a glass coverslip showed no detectable change in pipette position with applied hydrostatic pressure indicating that this does not alter the ion current. The relationship between the cantilever deformation and applied pressure was linear, with no hysteresis. This was also observed using pipettes of different resistance and hence inner radius. Since we know the spring constant of the cantilever, the distance moved by the cantilever can be directly converted into force using F= k (spring constant) x (distance) allowing a direct conversion of applied pressure into applied force. The force exerted on the cantilever should also depend on the applied pressure and pipette radius. The pipette radius, $R_{0,}$ can be calculated from the pipette resistance (Rp) using

$$Rp = 1/ (\pi \xi R_0 \tan\theta)$$

Where θ is the half cone angle of the inner wall of the pipette (1.5 degrees in our case) and ξ is the conductance of the solution. This formula was verified experimentally using scanning electron microscopy or optical microscopy of pipettes of measured resistance to directly determine $R_{0.}$ We then obtained a plot of the force exerted on the cantilever per kPa, for pipettes of different resistances.

Specifically, SICM has been used to explore the mechanical properties of cardiomyocytes with their characteristic repetitive scalloped topographic features.

The distance feedback control ensures that the pipette follows the indentation, which is a function of the applied pressure. This quantitatively probes the cell surface without direct contact. Knowing the effective force and distance one can determine a Young's Modulus of Elasticity. A hydraulic jet produces an initial small 200 nm indentation (Young's Modulus 1.3 kPa) followed by a larger indentation, with a larger Young's Modulus (2.8 kPa) (100). This component of the SICM not only probes mechanical properties of cells, but can also map any nano-heterogeneity in mechanical properties. A study in cardiomyocytes from heart failure shows changes in surface topography - Z grooves and t tubules (72) and the precise factors leading to this change are unclear.

8.3 Nano-Mechanotransduction and Mechanosensitivity

Mechanotransduction and mechanosensitivity is highly conserved and exists throughout biology (79). It involves mechanosensitive ion channels (29, 80), membrane and intracellular molecules, downstream intracellular signals and intracellular structures, including the cytoskeleton. Cellular mechanosensitivity is a burgeoning study area of rapidly increasing importance (39), particularly in heart (4, 10, 49, 56, 66, 118), and the vasculature (34, 48, 54, 82). The SICM was first used to study the mechanics of neurons (100) where a hydraulic jet could clearly indent the membrane. However, in cardiac myocytes a hydraulic jet (system diagrammed Figure 4C) can not only indent the membrane (Figure 4D – subthreshold pressure, left hand block arrow), but this indentation reached a threshold magnitude to activate contraction of the cardiomyocyte (65) (Figure 4D - threshold pressure right hand block arrow). That is, a mechanically induced potentially arrhythmogenic beat.

In an extended study (77) myocardial cells were loaded with Fluo-4 AM, a calcium sensitive dye. The SICM pipette initially scanned the cell membrane, with no applied

pipette pressure, producing a 3D image of membrane topology. Then pipette pressure is applied to selected coordinates, targeting crests, Z-grooves, or T-tubules. The jets indent the membrane activating a mechanosensitive calcium response, and these are determined by the cell's regional mechanical properties. The calcium response remains highly localized when pressure is applied over a groove, and spreads through the whole cell when the pressure is applied over a crest. The SICM has revealed the normal regular repetitive surface topography (see Figure 2A) of a myocardial cell, but cardiomyocytes from failing myocardium show surface disruption with no regular striations (see Figure 2E) and strikingly, hydraulic jets can generate an abnormal activating calcium signal regardless of the position of applied pressure.

8. General Perspectives and Conclusion

The nanopipette platform lends itself to label-free biosensing, using specific recognition compounds for analysis (19). For use in microinjection, it confers advantages over conventional techniques, with superior control over delivery, and the possible use of voltage instead of pressure to drive delivery. Thus more cells survive injection (the force produced by applying voltage across the liquid/liquid interface, which changes the surface tension, is enough to produce pipette flow). A few studies have provided results with this technique (8, 67, 91, 110). The SICM is not just a microscope as indicated in the left hand side of Figure 5. Because it uses a nanopipette as its scanning probe, it is a multifunctional convergent instrument (Figure 5 right hand side). It is a rapidly maturing technology. The potential of the "smart" patch-clamp method is yet to be fully explored. It can potentially be used to identify electrophysiological changes associated with morphological changes that occur in different circumstances, e.g. with cell differentiation from precursor cells (30). Moreover, combining "smart" patch-clamp and FRET-based signaling may

open new avenues of SICM application in cell physiology and pathology. An electron microscopic estimate of populations of membrane channels showed that stereo imaging is superior to non-stereo imaging for quantifying surface channels and receptors (62). Electron microscopy can provide a means of counting receptors and ion channels on freeze-fractured membranes. But because it uses freeze fracture, the number of functional channels cannot be estimated. Improved SICM scanning and electrophysiological procedures may provide accurate estimates of functional channels with nanometre precision.

Also, delivery through the pipette using pressure and/or voltage opens a host of possibilities (122). A multi-barrelled pipette can deliver multiple ligands such as agonists/inhibitors (98, 112). The SICM nano-pipette may be turned into highly sensitive electrochemical sensor, for spatiotemporal distribution of electrochemical mediators. The amount of substance released at different pressures and voltages can be calibrated and the release of chemicals from the pipette can be precisely controlled. By this, the nano-pipette can concentrate and control chemicals at the tip to trigger localized receptor mediated response opening the possibility of functional mapping of receptor mediated responses in cardiomyocytes and other biological cells. Local delivery enables replication in delivery of chemical agents to the same cellular structures at multiple points in the same dish without exposing neighbouring cells, or indeed other parts of the cell, to the drug. This could enable rapid drug testing experiments effectively at the nano-level that has not been possible previously.

The fact that the SICM uses a glass pipette for its probe, not only confers many purely biological applications (55), it is also useful in mechanobiology. In the latter case, force-based studies similar to that in the AFM (70), but noninvasively, will show whether the stiffness (Young’s Modulus of Elasticity) changes during

490 development, repair and regeneration, neoplasia, and heart pathology. Finally, the
491 pipette lends itself to sense probing, and nanofabrication.
492

References

1. **Allison DP, Mortensen NP, Sullivan CJ, and Doktycz MJ**. Atomic force microscopy of biological samples. *WileyInterdiscipRevNanomedNanobiotechnol* 2: 618-634, 2010.
2. **Azeloglu EU, and Costa KD**. Atomic force microscopy in mechanobiology: measuring microelastic heterogeneity of living cells. *Methods MolBiol* 736: 303-329, 2011.
3. **Baro AM, Miranda R, Alaman J, Garcia N, Binnig G, Rohrer H, Gerber C, and Carrascosa JL**. Determination of surface topography of biological specimens at high resolution by scanning tunnelling microscopy. *Nature* 315: 253-254, 1985.
4. **Baumgarten CM, Browe DM, and Ren Z**. Swelling- and Stretch-activated Chloride Channels in the Heart: Regulation and Function. 2005.
5. **Berridge MJ**. Calcium microdomains: organization and function. *Cell Calcium* 40: 405-412, 2006.
6. **Bers DM**. Cardiac excitation-contraction coupling. *Nature* 415: 198-205, 2002.
7. **Binnig G, Quate CF, and Gerber C**. Atomic force microscope. *PhysRevLett* 56: 930-933, 1986.
8. **Bruckbauer A, Zhou D, Ying L, Korchev YE, Abell C, and Klenerman D**. Multicomponent submicron features of biomolecules created by voltage controlled deposition from a nanopipet. *JAmChemSoc* 125: 9834-9839, 2003.
9. **Bustamante C, Vesenka J, Tang CL, Rees W, Guthold M, and Keller R**. Circular DNA molecules imaged in air by scanning force microscopy. *Biochemistry* 31: 22-26, 1992.

10. **Calaghan SC, and White E**. Mechanical Modulation of Intracellular Ion Concentrations: Mechanisms and Electrical Consequences. 2005.
11. **Calebiro D, Nikolaev VO, Persani L, and Lohse MJ**. Signaling by internalized G-protein-coupled receptors. *Trends PharmacolSci* 31: 221-228, 2010.
12. **Cheuk W, and Chan JK**. Subcellular localization of immunohistochemical signals: knowledge of the ultrastructural or biologic features of the antigens helps predict the signal localization and proper interpretation of immunostains. *IntJSurgPathol* 12: 185-206, 2004.
13. **Cho SJ, Wakade A, Pappas GD, and Jena BP**. New structure involved in transient membrane fusion and exocytosis. *AnnNYAcadSci* 971: 254-256, 2002.
14. **Colton RJ, Baselt DR, Dufrene YF, Green JB, and Lee GU**. Scanning probe microscopy. *CurrOpinChemBiol* 1: 370-377, 1997.
15. **Cong Y, and Ludtke SJ**. Single particle analysis at high resolution. *Methods Enzymol* 482: 211-235, 2010.
16. **Crowe WE, Ehrenfeld J, Brochiero E, and Wills NK**. Apical membrane sodium and chloride entry during osmotic swelling of renal (A6) epithelial cells. *JMembrBiol* 144: 81-91, 1995.
17. **Dai J, and Sheetz MP**. Mechanical properties of neuronal growth cone membranes studied by tether formation with laser optical tweezers. *BiophysJ* 68: 988-996, 1995.
18. **de Jonge N, Peckys DB, Kremers GJ, and Piston DW**. Electron microscopy of whole cells in liquid with nanometer resolution. *Proceedings of the National Academy of Sciences of the United States of America* 106: 2159-2164, 2009.

19. **Ding S, Gao C, and Gu LQ**. Capturing single molecules of immunoglobulin and ricin with an aptamer-encoded glass nanopore. *AnalChem* 81: 6649-6655, 2009.

20. **Domke KF, and Pettinger B**. Studying surface chemistry beyond the diffraction limit: 10 years of TERS. *Chemphyschem* 11: 1365-1373, 2010.

21. **Dufrene YF, Boonaert CJP, van der Mei HC, Busscher HJ, and Rouxhet PG**. Probing molecular interactions and mechanical properties of microbial cell surfaces by atomic force microscopy. *Ultramicroscopy* 86: 113-120, 2001.

22. **Dulinska I, Targosz M, Strojny W, Lekka M, Czuba P, Balwierz W, and Szymonski M**. Stiffness of normal and pathological erythrocytes studied by means of atomic force microscopy. *JBiochemBiophysMethods* 66: 1-11, 2006.

23. **Duman M, Pfleger M, Zhu R, Rankl C, Chtcheglova LA, Neundlinger I, Bozna BL, Mayer B, Salio M, Shepherd D, Polzella P, Moertelmaier M, Kada G, Ebner A, Dieudonne M, Schutz GJ, Cerundolo V, Kienberger F, and Hinterdorfer P**. Improved localization of cellular membrane receptors using combined fluorescence microscopy and simultaneous topography and recognition imaging. *Nanotechnology* 21: 115504, 2010.

24. **Dutta AK, Korchev YE, Shevchuk AI, Hayashi S, Okada Y, and Sabirov RZ**. Spatial distribution of maxi-anion channel on cardiomyocytes detected by smart-patch technique. *BiophysJ* 94: 1646-1655, 2008.

25. **Errington RJ, Fricker MD, Wood JL, Hall AC, and White NS**. Four-dimensional imaging of living chondrocytes in cartilage using confocal microscopy: a pragmatic approach. *AmJPhysiol* 272: C1040-C1051, 1997.

26. **Farinas J, Kneen M, Moore M, and Verkman AS**. Plasma membrane water permeability of cultured cells and epithelia measured by light microscopy with spatial filtering. *JGenPhysiol* 110: 283-296, 1997.

27. **Francis LW, Lewis PD, Wright CJ, and Conlan RS**. Atomic force microscopy comes of age. *BiolCell* 102: 133-143, 2010.

28. **Frederix PL, Bosshart PD, and Engel A**. Atomic force microscopy of biological membranes. *BiophysJ* 96: 329-338, 2009.

29. **French AS**. Mechanotransduction. *Annual review of physiology* 54: 135-152, 1992.

30. **Gorelik J, Ali NN, Sheikh Abdul Kadir SH, Lab M, Stojkovic P, Armstrong L, Sviderskaya EV, Negulyaev YA, Klenerman D, Bennett DC, Lako M, Harding SE, Stojkovic M, and Korchev YE**. Non-invasive imaging of stem cells by scanning ion conductance microscopy: future perspective. *Tissue Eng Part CMethods* 14: 311-318, 2008.

31. **Gorelik J, Gu Y, Spohr HA, Shevchuk AI, Lab MJ, Harding SE, Edwards CR, Whitaker M, Moss GW, Benton DC, Sanchez D, Darszon A, Vodyanoy I, Klenerman D, and Korchev YE**. Ion channels in small cells and subcellular structures can be studied with a smart patch-clamp system. *BiophysJ* 83: 3296-3303, 2002.

32. **Gorelik J, Shevchuk AI, Frolenkov GI, Diakonov IA, Lab MJ, Kros CJ, Richardson GP, Vodyanoy I, Edwards CR, Klenerman D, and Korchev YE**. Dynamic assembly of surface structures in living cells. *ProcNatlAcadSciUSA* 100: 5819-5822, 2003.

33. **Grashoff C, Hoffman BD, Brenner MD, Zhou R, Parsons M, Yang MT, McLean MA, Sligar SG, Chen CS, Ha T, and Schwartz MA**. Measuring mechanical tension across vinculin reveals regulation of focal adhesion dynamics. *Nature* 466: 263-266, 2010.

34. **Groschner K**. Two ways to feel the pressure: an endothelial Ca(2+) entry channel with dual mechanosensitivity. *CardiovascRes* 53: 9-11, 2002.

35. **Gu Y, Gorelik J, Spohr HA, Shevchuk A, Lab MJ, Harding SE, Vodyanoy I, Klenerman D, and Korchev YE**. High-resolution scanning patch-clamp: new insights into cell function. *FASEB J* 16: 748-750, 2002.

36. **Guilak F**. Volume and surface area measurement of viable chondrocytes in situ using geometric modelling of serial confocal sections. *JMicrosc* 173: 245-256, 1994.

37. **Haga H, Sasaki S, Kawabata K, Ito E, Ushiki T, and Sambongi T**. Elasticity mapping of living fibroblasts by AFM and immunofluorescence observation of the cytoskeleton. *Ultramicroscopy* 82: 253-258, 2000.

38. **Hallows KR, Law FY, Packman CH, and Knauf PA**. Changes in cytoskeletal actin content, F-actin distribution, and surface morphology during HL-60 cell volume regulation. *JCell Physiol* 167: 60-71, 1996.

39. **Hamill OP**. Twenty odd years of stretch-sensitive channels. *Pflugers Arch* 453: 333-351, 2006.

40. **Hansma PK, Drake B, Marti O, Gould SA, and Prater CB**. The scanning ion-conductance microscope. *Science* 243: 641-643, 1989.

41. **Hawes C, and Martin B**. Freeze-fracture deep-etch methods. *Methods Cell Biol* 49: 33-43, 1995.

42. **Haydon PG, Lartius R, Parpura V, and Marchese-Ragona SP**. Membrane deformation of living glial cells using atomic force microscopy. *JMicrosc* 182: 114-120, 1996.

43. **Hisatsune C, and Mikoshiba K**. Novel compartment implicated in calcium signaling--is it an "induced coupling domain"? *SciSTKE* 2005: e53, 2005.

44. **Hochmuth RM**. Micropipette aspiration of living cells. *JBiomech* 33: 15-22, 2000.

620 45. **Hoffmann EK**. Cell swelling and volume regulation. *CanJPhysiol Pharmacol* 70
621 Suppl: S310-S313, 1992.
622 46. **Horber JK, and Miles MJ**. Scanning probe evolution in biology. *Science* 302:
623 1002-1005, 2003.
624 47. **Hur EM, and Kim KT**. G protein-coupled receptor signalling and cross-talk:
625 achieving rapidity and specificity. *Cell Signal* 14: 397-405, 2002.
626 48. **Inoue R, Jian Z, and Kawarabayashi Y**. Mechanosensitive TRP channels in
627 cardiovascular pathophysiology. *PharmacolTher* 123: 371-385, 2009.
628 49. **Isenberg G, Kazanski V, Kondratev D, Gallitelli MF, Kiseleva I, and**
629 **Kamkin A**. Differential effects of stretch and compression on membrane
630 currents and [Na+]c in ventricular myocytes. *ProgBiophysMolBiol* 82: 43-56,
631 2003.
632 50. **Jacot JG, Dianis S, Schnall J, and Wong JY**. A simple microindentation
633 technique for mapping the microscale compliance of soft hydrated materials
634 and tissues. *JBiomedMaterResA* 79: 485-494, 2006.
635 51. **Janmey PA, Winer JP, Murray ME, and Wen Q**. The hard life of soft cells.
636 *Cell MotilCytoskeleton* 66: 597-605, 2009.
637 52. **Karoutsos V**. Scanning probe microscopy: instrumentation and applications
638 on thin films and magnetic multilayers. *JNanosciNanotechnol* 9: 6783-6798,
639 2009.
640 53. **Kawahara K, Onodera M, and Fukuda Y**. A simple method for continuous
641 measurement of cell height during a volume change in a single A6 cell.
642 *JpnJPhysiol* 44: 411-419, 1994.
643 54. **Khayutin VM, Lukoshkova EV, Rogoza AN, and Nikolsky VP**. Negative
644 feedbacks in the pathogenesis of primary arterial hypertension:
645 mechanosensitivity of the endothelium. *Blood Press* 4: 70-76, 1995.

55. **Klenerman D, and Korchev Y**. Potential biomedical applications of the scanned nanopipette. *Nanomedicine(Lond)* 1: 107-114, 2006.

56. **Kohl P, Camelliti P, Burton FL, and Smith GL**. Electrical coupling of fibroblasts and myocytes: relevance for cardiac propagation. *JElectrocardiol* 38: 45-50, 2005.

57. **Korchev YE, Bashford CL, Milovanovic M, Vodyanoy I, and Lab MJ**. Scanning ion conductance microscopy of living cells. *BiophysJ* 73: 653-658, 1997.

58. **Korchev YE, Gorelik J, Lab MJ, Sviderskaya EV, Johnston CL, Coombes CR, Vodyanoy I, and Edwards CR**. Cell volume measurement using scanning ion conductance microscopy. *BiophysJ* 78: 451-457, 2000.

59. **Korchev YE, Milovanovic M, Bashford CL, Bennett DC, Sviderskaya EV, Vodyanoy I, and Lab MJ**. Specialized scanning ion-conductance microscope for imaging of living cells. *JMicrosc* 188: 17-23, 1997.

60. **Korchev YE, Negulyaev YA, Edwards CR, Vodyanoy I, and Lab MJ**. Functional localization of single active ion channels on the surface of a living cell. *NatCell Biol* 2: 616-619, 2000.

61. **Korchev YE, Raval M, Lab MJ, Gorelik J, Edwards CR, Rayment T, and Klenerman D**. Hybrid scanning ion conductance and scanning near-field optical microscopy for the study of living cells. *BiophysJ* 78: 2675-2679, 2000.

62. **Kordylewski L, Karrison T, and Page E**. P-face particle density of freeze-fractured vertebrate cardiac plasma membrane. *AmJPhysiol* 245: H992-H997, 1983.

63. **Kurachi Y, and Ishii M**. Cell signal control of the G protein-gated potassium channel and its subcellular localization. *JPhysiol* 554: 285-294, 2004.

64. **Kuznetsova TG, Starodubtseva MN, Yegorenkov NI, Chizhik SA, and Zhdanov RI**. Atomic force microscopy probing of cell elasticity. *Micron* 38: 824-833, 2007.

65. **Lab M**. Scanning Ion Conductance Microscopy for Imaging and Mechanosensitive Activation of Selected Areas of Live Cells. *Mechanosensitivity of the Heart* 3: 6, 2012.

66. **Lab MJ**. Mechanically Mediated Crosstalk in Heart. 2005.

67. **Laforge FO, Carpino J, Rotenberg SA, and Mirkin MV**. Electrochemical attosyringe. *ProcNatlAcadSciUSA* 104: 11895-11900, 2007.

68. **Lekka M, Fornal M, Pyka-Fosciak G, Lebed K, Wizner B, Grodzicki T, and Styczen J**. Erythrocyte stiffness probed using atomic force microscope. *Biorheology* 42: 307-317, 2005.

69. **Lesniewska E, Giocondi MC, Vie V, Finot E, Goudonnet JP, and Le GC**. Atomic force microscopy of renal cells: limits and prospects. *Kidney IntSuppl* 65: S42-S48, 1998.

70. **Liu Y, Feng J, Shi L, Niu R, Sun Q, Liu H, Li J, Guo J, Zhu J, and Han D**. In situ mechanical analysis of cardiomyocytes at nano scales. *Nanoscale* 4: 99-102, 2012.

71. **Ludwig T, Kirmse R, Poole K, and Schwarz US**. Probing cellular microenvironments and tissue remodeling by atomic force microscopy. *Pflugers Arch* 456: 29-49, 2008.

72. **Lyon AR, Macleod KT, Zhang Y, Garcia E, Kanda GK, Lab MJ, Korchev YE, Harding SE, and Gorelik J**. Loss of T-tubules and other changes to surface topography in ventricular myocytes from failing human and rat heart. *ProcNatlAcadSciUSA* 106: 6854-6859, 2009.

73. **Mader A, Gruber K, Castelli R, Hermann BA, Seeberger PH, Radler JO, and Leisner M**. Discrimination of Escherichia coli strains using glycan cantilever array sensors. *NanoLett* 12: 420-423, 2012.

74. **Manley S, Gillette JM, Patterson GH, Shroff H, Hess HF, Betzig E, and Lippincott-Schwartz J**. High-density mapping of single-molecule trajectories with photoactivated localization microscopy. *NatMethods* 5: 155-157, 2008.

75. **McManus ML, and Strange K**. Acute volume regulation of brain cells in response to hypertonic challenge. *Anesthesiology* 78: 1132-1137, 1993.

76. **Meyer HW, and Richter W**. Freeze-fracture studies on lipids and membranes. *Micron* 32: 615-644, 2001.

77. **Miragoli M, Lab MJ, Sikkel M, Lyon AR, and Gorelik J**. Structural Remodeling in Cardiomyocytes from Infarcted Hearts Potentiates Cellular Mechano Arrhythmic response to Nanoscale Sarcolemmal Perturbation. *Circulation Meeting abstract* 124: 2011.

78. **Mitsuoka K**. Obtaining high-resolution images of biological macromolecules by using a cryo-electron microscope with a liquid-helium cooled stage. *Micron* 42: 100-106, 2011.

79. **Moe PC, Blount P, and Kung C**. Functional and structural conservation in the mechanosensitive channel MscL implicates elements crucial for mechanosensation. *MolMicrobiol* 28: 583-592, 1998.

80. **Morris CE**. Mechanosensitive ion channels. *JMembrBiol* 113: 93-107, 1990.

81. **Muller DJ, Helenius J, Alsteens D, and Dufrene YF**. Force probing surfaces of living cells to molecular resolution. *Nature chemical biology* 5: 383-390, 2009.

82. **Muraki K, Shigekawa M, and Imaizumi Y**. A New Insight into the Function of TRPV2 in Circulatory Organs. 2007.

722 83. **Myhra S**. A review of enabling technologies based on scanning probe
723 microscopy relevant to bioanalysis. *BiosensBioelectron* 19: 1345-1354, 2004.
724 84. **Nakahari T, Murakami M, Yoshida H, Miyamoto M, Sohma Y, and Imai**
725 **Y**. Decrease in rat submandibular acinar cell volume during ACh stimulation.
726 *AmJPhysiol* 258: G878-G886, 1990.
727 85. **Nikolaev VO, Moshkov A, Lyon AR, Miragoli M, Novak P, Paur H, Lohse**
728 **MJ, Korchev YE, Harding SE, and Gorelik J**. Beta2-adrenergic receptor
729 redistribution in heart failure changes cAMP compartmentation. *Science* 327:
730 1653-1657, 2010.
731 86. **Novak P, Li C, Shevchuk AI, Stepanyan R, Caldwell M, Hughes S, Smart**
732 **TG, Gorelik J, Ostanin VP, Lab MJ, Moss GW, Frolenkov GI, Klenerman**
733 **D, and Korchev YE**. Nanoscale live-cell imaging using hopping probe ion
734 conductance microscopy. *NatMethods* 6: 279-281, 2009.
735 87. **Oberleithner H**. Nanophysiology: fact or fiction? *Pflugers Archiv : European*
736 *journal of physiology* 456: 1-2, 2008.
737 88. **Orchard C, and Brette F**. t-Tubules and sarcoplasmic reticulum function in
738 cardiac ventricular myocytes. *CardiovascRes* 77: 237-244, 2008.
739 89. **Papp S, Dziak E, Michalak M, and Opas M**. Is all of the endoplasmic
740 reticulum created equal? The effects of the heterogeneous distribution of
741 endoplasmic reticulum Ca2+-handling proteins. *JCell Biol* 160: 475-479, 2003.
742 90. **Peyton SR, Ghajar CM, Khatiwala CB, and Putnam AJ**. The emergence of
743 ECM mechanics and cytoskeletal tension as important regulators of cell
744 function. *Cell BiochemBiophys* 47: 300-320, 2007.
745 91. **Piper JD, Clarke RW, Korchev YE, Ying L, and Klenerman D**. A renewable
746 nanosensor based on a glass nanopipette. *JAmChemSoc* 128: 16462-16463,
747 2006.

92. **Poggi MA, Gadsby ED, Bottomley LA, King WP, Oroudjev E, and Hansma H**. Scanning probe microscopy. *AnalChem* 76: 3429-3443, 2004.

93. **Potter CM, Schobesberger S, Lundberg MH, Weinberg PD, Mitchell JA, and Gorelik J**. Shape and compliance of endothelial cells after shear stress in vitro or from different aortic regions: scanning ion conductance microscopy study. *PLoSOne* 7: e31228, 2012.

94. **Quist AP, Bergman AA, Reimann CT, Oscarsson SO, and Sundqvist BU**. Imaging of single antigens, antibodies, and specific immunocomplex formation by scanning force microscopy. *Scanning Microsc* 9: 395-400, 1995.

95. **Ramachandran S, Teran AF, and Lal R**. Potential role of atomic force microscopy in systems biology. *WileyInterdiscipRevSystBiolMed* 3: 702-716, 2011.

96. **Rheinlaender J, Geisse NA, Proksch R, and Schaffer TE**. Comparison of scanning ion conductance microscopy with atomic force microscopy for cell imaging. *Langmuir* 27: 697-704, 2011.

97. **Rheinlaender J, and Schaffer TE**. Image formation, resolution, and height measurement in scanning ion conductance microscopy. *J Appl Phys* 105: 9, 2009

98. **Rodolfa KT, Bruckbauer A, Zhou D, Korchev YE, and Klenerman D**. Two-component graded deposition of biomolecules with a double-barreled nanopipette. *AngewChemIntEd Engl* 44: 6854-6859, 2005.

99. **Rotsch C, Braet F, Wisse E, and Radmacher M**. AFM imaging and elasticity measurements on living rat liver macrophages. *Cell BiolInt* 21: 685-696, 1997.

100. **Sanchez D, Johnson N, Li C, Novak P, Rheinlaender J, Zhang Y, Anand U, Anand P, Gorelik J, Frolenkov GI, Benham C, Lab M, Ostanin VP,**

Schaffer TE, Klenerman D, and Korchev YE. Noncontact measurement of the local mechanical properties of living cells using pressure applied via a pipette. *BiophysJ* 95: 3017-3027, 2008.

101. **Schermelleh L, Heintzmann R, and Leonhardt H**. A guide to super-resolution fluorescence microscopy. *The Journal of cell biology* 190: 165-175, 2010.
102. **Scott JD**. A-kinase-anchoring proteins and cytoskeletal signalling events. *BiochemSocTrans* 31: 87-89, 2003.
103. **Sen S, Subramanian S, and Discher DE**. Indentation and adhesive probing of a cell membrane with AFM: theoretical model and experiments. *BiophysJ* 89: 3203-3213, 2005.
104. **Shevchuk AI, Frolenkov GI, Sanchez D, James PS, Freedman N, Lab MJ, Jones R, Klenerman D, and Korchev YE**. Imaging proteins in membranes of living cells by high-resolution scanning ion conductance microscopy. *AngewChemIntEd Engl* 45: 2212-2216, 2006.
105. **Shevchuk AI, Hobson P, Lab MJ, Klenerman D, Krauzewicz N, and Korchev YE**. Endocytic pathways: combined scanning ion conductance and surface confocal microscopy study. *Pflugers Arch* 456: 227-235, 2008.
106. **Shevchuk AI, Hobson P, Lab MJ, Klenerman D, Krauzewicz N, and Korchev YE**. Imaging single virus particles on the surface of cell membranes by high-resolution scanning surface confocal microscopy. *BiophysJ* 94: 4089-4094, 2008.
107. **Shevchuk AI, Novak P, Takahashi Y, Clarke R, Miragoli M, Babakinejad B, Gorelik J, Korchev YE, and Klenerman D**. Realizing the biological and biomedical potential of nanoscale imaging using a pipette probe. *Nanomedicine(Lond)* 6: 565-575, 2011.

800 108. **Stewart MP, Toyoda Y, Hyman AA, and Muller DJ**. Force probing cell
801 shape changes to molecular resolution. *Trends BiochemSci* 36: 444-450,
802 2011.
803 109. **Stolz M, Raiteri R, Daniels AU, VanLandingham MR, Baschong W, and**
804 **Aebi U**. Dynamic elastic modulus of porcine articular cartilage determined at
805 two different levels of tissue organization by indentation-type atomic force
806 microscopy. *BiophysJ* 86: 3269-3283, 2004.
807 110. **Sun HW, and Suo R**. [Investigation of enhancing effect for hydride
808 generation-atomic fluorescence of transition metal elements]. *GuangPuXueYu*
809 *GuangPuFenXi* 28: 2684-2690, 2008.
810 111. **Svoboda K, and Block SM**. Biological applications of optical forces.
811 *AnnuRevBiophysBiomolStruct* 23: 247-285, 1994.
812 112. **Takahashi Y, Shevchuk AI, Novak P, Zhang Y, Ebejer N, Macpherson**
813 **JV, Unwin PR, Pollard AJ, Roy D, Clifford CA, Shiku H, Matsue T,**
814 **Klenerman D, and Korchev YE**. Multifunctional nanoprobes for nanoscale
815 chemical imaging and localized chemical delivery at surfaces and interfaces.
816 *AngewChemIntEd Engl* 50: 9638-9642, 2011.
817 113. **te RJ, Katan AJ, Rankl C, Stahl SW, van Buul AM, Phang IY, Gomez-**
818 **Casado A, Schon P, Gerritsen JW, Cambi A, Rowan AE, Vancso GJ,**
819 **Jonkheijm P, Huskens J, Oosterkamp TH, Gaub H, Hinterdorfer P,**
820 **Figdor CG, and Speller S**. Interlaboratory round robin on cantilever
821 calibration for AFM force spectroscopy. *Ultramicroscopy* 111: 1659-1669,
822 2011.
823 114. **Tosolini G, Villanueva LG, Perez-Murano F, and Bausells J**. Fast on-wafer
824 electrical, mechanical, and electromechanical characterization of piezoresistive
825 cantilever force sensors. *RevSciInstrum* 83: 015002, 2012.

826 115. **Turner YT, Roberts CJ, and Davies MC**. Scanning probe microscopy in the
827 field of drug delivery. *AdvDrug DelivRev* 59: 1453-1473, 2007.
828 116. **van de Linde S, Loschberger A, Klein T, Heidbreder M, Wolter S,**
829 **Heilemann M, and Sauer M**. Direct stochastic optical reconstruction
830 microscopy with standard fluorescent probes. *Nature protocols* 6: 991-1009,
831 2011.
832 117. **Webb HK, Truong VK, Hasan J, Crawford RJ, and Ivanova EP**. Physico-
833 mechanical characterisation of cells using atomic force microscopy - Current
834 research and methodologies. *JMicrobiolMethods* 86: 131-139, 2011.
835 118. **White E**. Mechanosensitive channels: therapeutic targets in the myocardium?
836 *CurrPharmDes* 12: 3645-3663, 2006.
837 119. **Willig KI, Kellner RR, Medda R, Hein B, Jakobs S, and Hell SW**.
838 Nanoscale resolution in GFP-based microscopy. *NatMethods* 3: 721-723, 2006.
839 120. **Wozniak M, Keefer JR, Saunders C, and Limbird LE**. Differential targeting
840 and retention of G protein-coupled receptors in polarized epithelial cells.
841 *JReceptSignalTransductRes* 17: 373-383, 1997.
842 121. **Xu LP, Liu Y, and Zhang X**. Interfacial self-assembly of amino acids and
843 peptides: scanning tunneling microscopy investigation. *Nanoscale* 3: 4901-
844 4915, 2011.
845 122. **Ying L, Bruckbauer A, Zhou D, Gorelik J, Shevchuk A, Lab M, Korchev**
846 **Y, and Klenerman D**. The scanned nanopipette: a new tool for high
847 resolution bioimaging and controlled deposition of biomolecules.
848 *PhysChemChemPhys* 7: 2859-2866, 2005.
849 123. **You HX, Lau JM, Zhang S, and Yu L**. Atomic force microscopy imaging of
850 living cells: a preliminary study of the disruptive effect of the cantilever tip on
851 cell morphology. *Ultramicroscopy* 82: 297-305, 2000.

124. **Yu H, Yang T, Chen Y, Xu P, Lee DW, and Li X**. Chemo-mechanical joint detection with both dynamic and static microcantilevers for interhomologue molecular identification. *AnalChem* 84: 6679-6685, 2012.

125. **Zhang Y, Gorelik J, Sanchez D, Shevchuk A, Lab M, Vodyanoy I, Klenerman D, Edwards C, and Korchev Y**. Scanning ion conductance microscopy reveals how a functional renal epithelial monolayer maintains its integrity. *Kidney Int* 68: 1071-1077, 2005.

126. **Zhu J, Sabharwal T, Kalyanasundaram A, Guo L, and Wang G**. Topographic mapping and compression elasticity analysis of skinned cardiac muscle fibers in vitro with atomic force microscopy and nanoindentation. *JBiomech* 42: 2143-2150, 2009.

127. **Zhu Q, Tekola P, Baak JP, and Belien JA**. Measurement by confocal laser scanning microscopy of the volume of epidermal nuclei in thick skin sections. *AnalQuantCytolHistol* 16: 145-152, 1994.

Figure Legends

Figure 1. Schematic diagram of Scanning Ion Conductance Microscope (SICM). The electrolyte-filled scanning nanopipette is mounted on a piezo translation platform. It also contains an Ag/AgCl electrode connected to an ion current detector/amplifier above. The input to this detector is an ion current signal from the bath (left hand side vertical line). The amplifier's output drives a feedback control amplifier (right hand side vertical line) to control the pipette's piezo, which provides a Z only directional movement (up and down). It also provides a drive to the nanopositioning stage (bottom) but raster scanning in two directions (X Y). An optical system under the nanopositioning stage focuses a laser to a confocal volume near the pipette's tip, and also provides the required detection system.

Figure 2. Functional localization of βAR-induced cAMP signaling and the principle of the combined nanoscale SICM-FRET approach. A) SICM surface image indicating the positioning of the pipette, and diagramming isoprenaline (ISO) application. **B)** Scheme of receptor activity measured by monitoring the production of cAMP by Epac2-camps, a FRET-based cAMP sensor that changes its conformation and fluorescence properties upon activation—i.e.cAMP binding. YFP and CFP, yellow and cyan fluorescent proteins, respectively. **C)** Healthy cardiomyocyte with a well-defined surface topography showing its regular surface structure. Z grooves separating crests provide a scalloped surface, with T tubules visible in the grooves – good Z groove index – see text. **D)** FRET ratio on application of ISO to T-tubule or crest in healthy myocardium. A response was only recorded in the T-tubular regions suggesting the β_2AR is preferentially localized here. **E)** Cardiomyocyte from a rat with myocardial failure, showing a disrupted surface topography. There is no clear

relation between T tubules and Z grooves - poor Z groove index. **F)** ISO application produces cAMP signals both in T-tubules and crest suggesting the loss of cAMP compartmentation in heart failure.

Figure 3. L type calcium channel (**LTCC) distribution in the cardiomyocyte membrane: mapping of ion channels by the "smart" patch-clamp technique. A)** Adult rat cardiomyocyte and micropipette as seen by optical microscope. **B)** Diagram of smart patch circuitry with vertical pipette. **C)** Cardiomyocyte topography showing the regular Z grooves and crests (scalloped surface) with T-tubules **D)** Schematic of myocyte cross-section with probe positioning in sarcomere units (Z-groove, T-tubule opening and scallop crest). Probabilities of forming a GΩ seal as a function of surface position are shown in parenthesis. **E)** Cell-attached Ba^{2+} currents at 0 mV showing several current traces and ensemble average of 12 traces showing typical LTCC current kinetics. **F)** Diagrammatic representation of statistical distribution of LTCCs with the highest density near the T-tubule opening. Modified from (35) with permission.

Figure 4. Vertical (Z) Deflection and Signal Detection. (A). Diagram of vertical displacement (contraction) measure and illumination with calcium detection. The SICM pipette hovers above the myocyte. Its contraction is represented by the relaxed myocyte (grey dotted outline) contracting inwards and downwards (indicated by diagonal dashed arrows) to the contracted state of the myocyte (solid outline). This contraction displaces the horizontal platform up and down (Z deflection). Confocal illumination is from below, focussing on a confocal volume beneath the myocyte membrane (small red rectangle). (B). Traces of digitised Z deflection (left ordinate - contraction) is in black, with the calcium signal

in red (right ordinate). (C) Cardiomyocyte with diagrammed pipette applying pressure in system with similar setup to (A). Pressure source ejects fluid from pipette tip to indent cardiomyocyte membrane surface. (D) Subthreshold pressure stimulation (left block arrow) produces a small indentation of about 0.5 μm (upward deflection in height), whereas a higher threshold pressure (right block arrow) not only produces a larger indentation, but elicits a contraction (sharpish upward deflection

Figure 5 Summary Diagram of overall functionality of the Scanning Ion Conductance Microscope (SICM). The pipette can function as various probes (input to central SICM sphere from below.) The spokes radiating out from the SICM sphere reach towards other spheres, which indicate the range of functionality. The spheres on the left sub-serve its original and basic function as a microscope. It can image large molecules through to a whole cell. The spheres on the right motion the SICM's diverse hybrid function – the top two spheres, signal and electrophysiological surface location (ion channels, receptors), and the bottom two – mechanical.

Table Legend

Table 1. Resolutions of microscopy techniques. Abbreviations – nm = nanometer; SICM = Scanning Ion Conductance Microscope; SEM = Scanning Electron Microscope; TEM = Transmission Electron Microscope; AFM = Atomic Force Microscope. ***Not ideal for cell surfaces**

Figure 1

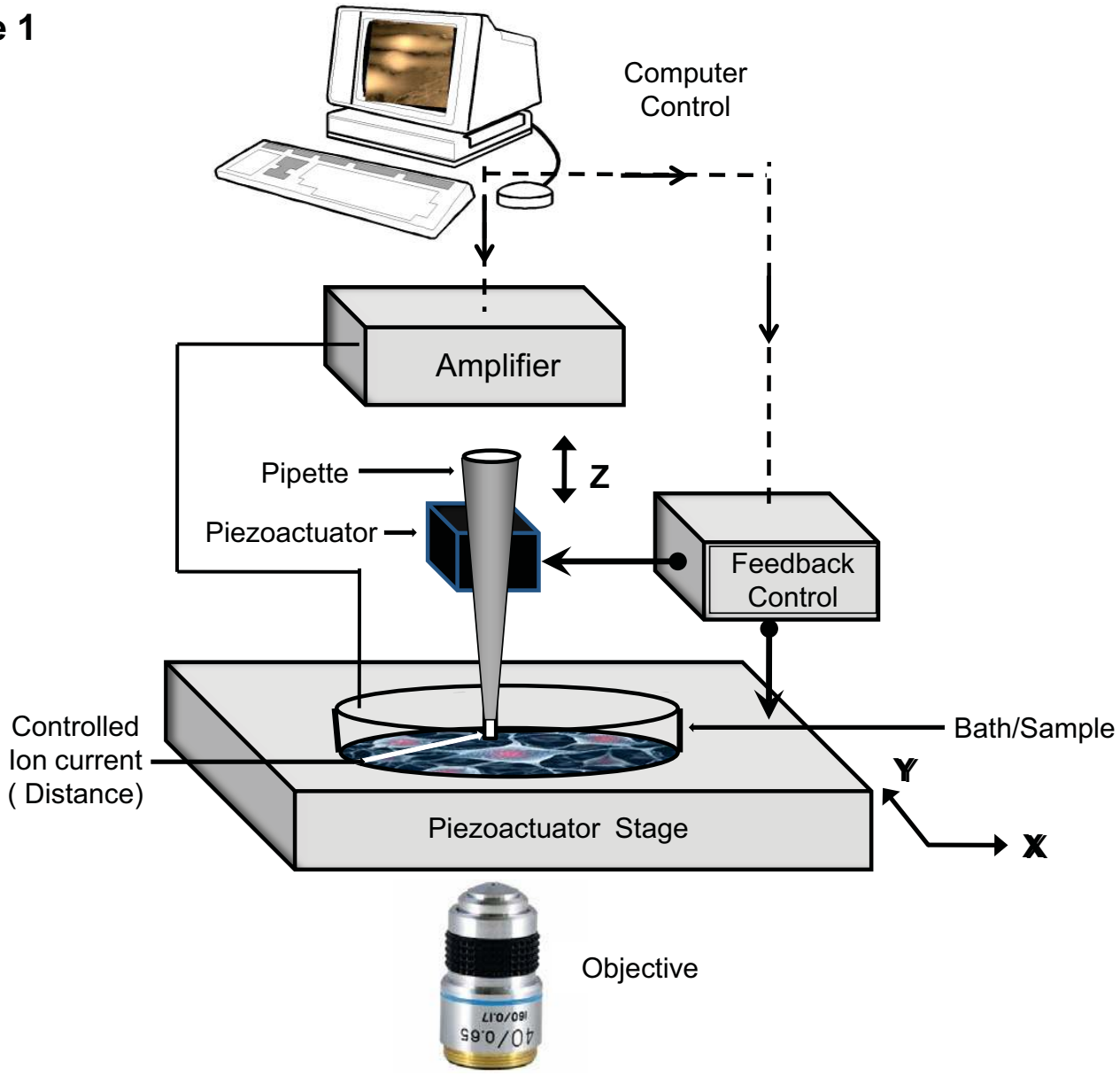
Computer
Control
Amplifier
Pipette
Z
Piezoactuator
Feedback
Control
Controlled
Ion current
(Distance)
Bath/Sample
Y
X
Piezoactuator Stage
Objective

Figure 2

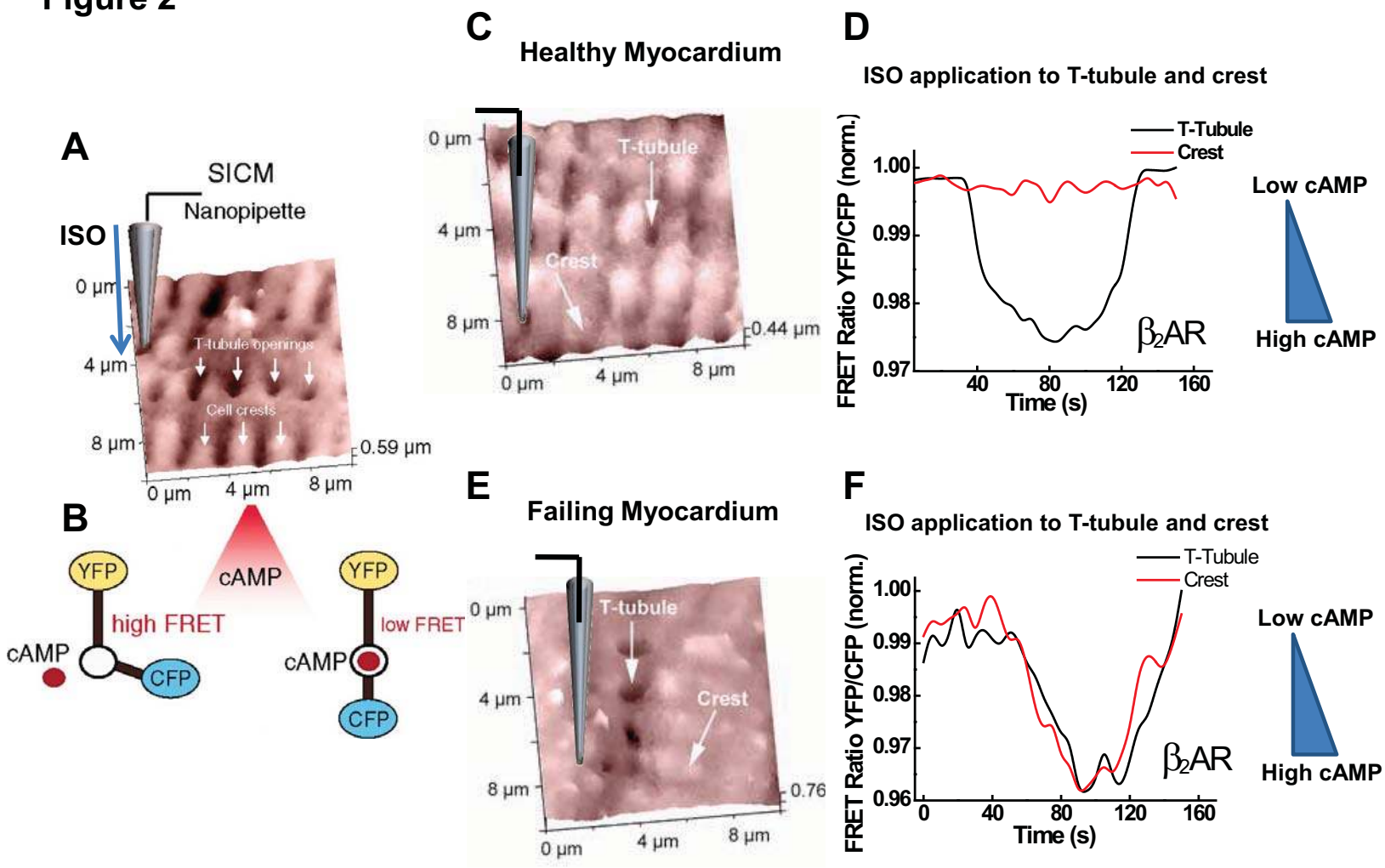
A
SICM
Nanopipette
ISO
0 µm
4 µm
8 µm
T-tubule openings
Cell crests
0.59 µm
0 µm
4 µm
8 µm
B
YFP
cAMP
high FRET
CFP
cAMP
YFP
low FRET
cAMP
CFP
C
Healthy Myocardium
0 µm
4 µm
8 µm
T-tubule
Crest
0.44 µm
0 µm
4 µm
8 µm
D
ISO application to T-tubule and crest
FRET Ratio YFP/CFP (norm.)
1.00
0.99
0.98
0.97
T-Tubule
Crest
β2AR
40
80
120
160
Time (s)
Low cAMP
High cAMP
E
Failing Myocardium
0 µm
4 µm
8 µm
T-tubule
Crest
0.76
0 µm
4 µm
8 µm
F
ISO application to T-tubule and crest
FRET Ratio YFP/CFP (norm.)
1.00
0.99
0.98
0.97
0.96
T-Tubule
Crest
β2AR
0
40
80
120
160
Time (s)
Low cAMP
High cAMP

Figure 3

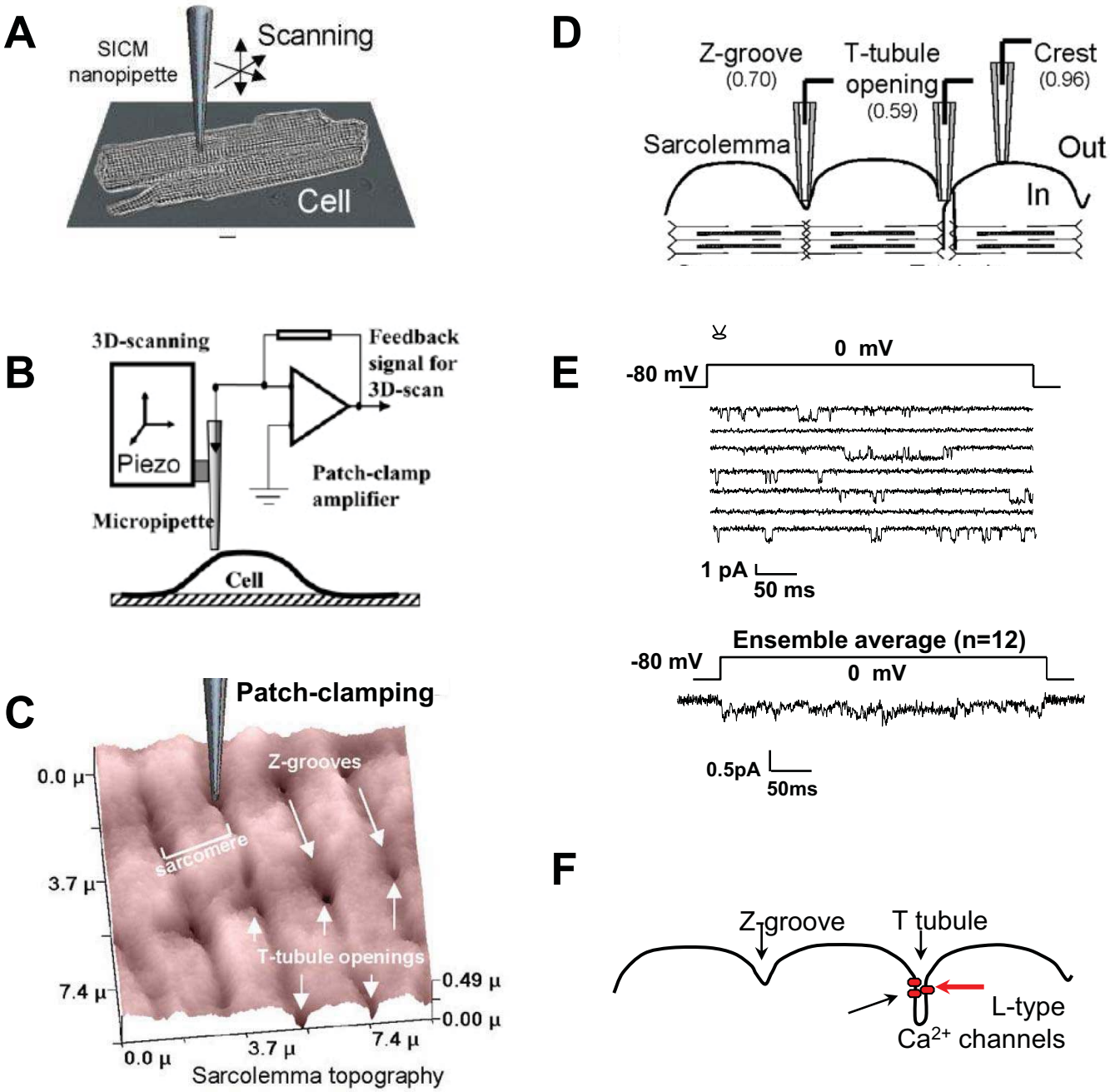
A
SICM
nanopipette
Scanning
Cell
B
3D-scanning
Feedback
signal for
3D-scan
Piezo
Patch-clamp
amplifier
Micropipette
Cell
C
Patch-clamping
Z-grooves
sarcomere
T-tubule openings
0.0 µ
3.7 µ
7.4 µ
0.49 µ
0.00 µ
0.0 µ
3.7 µ
7.4 µ
Sarcolemma topography
D
Z-groove
(0.70)
T-tubule
opening
(0.59)
Crest
(0.96)
Sarcolemma
Out
In
E
0 mV
-80 mV
1 pA
50 ms
Ensemble average (n=12)
-80 mV
0 mV
0.5pA
50ms
F
Z-groove
T tubule
L-type
Ca2+ channels

Figure 4

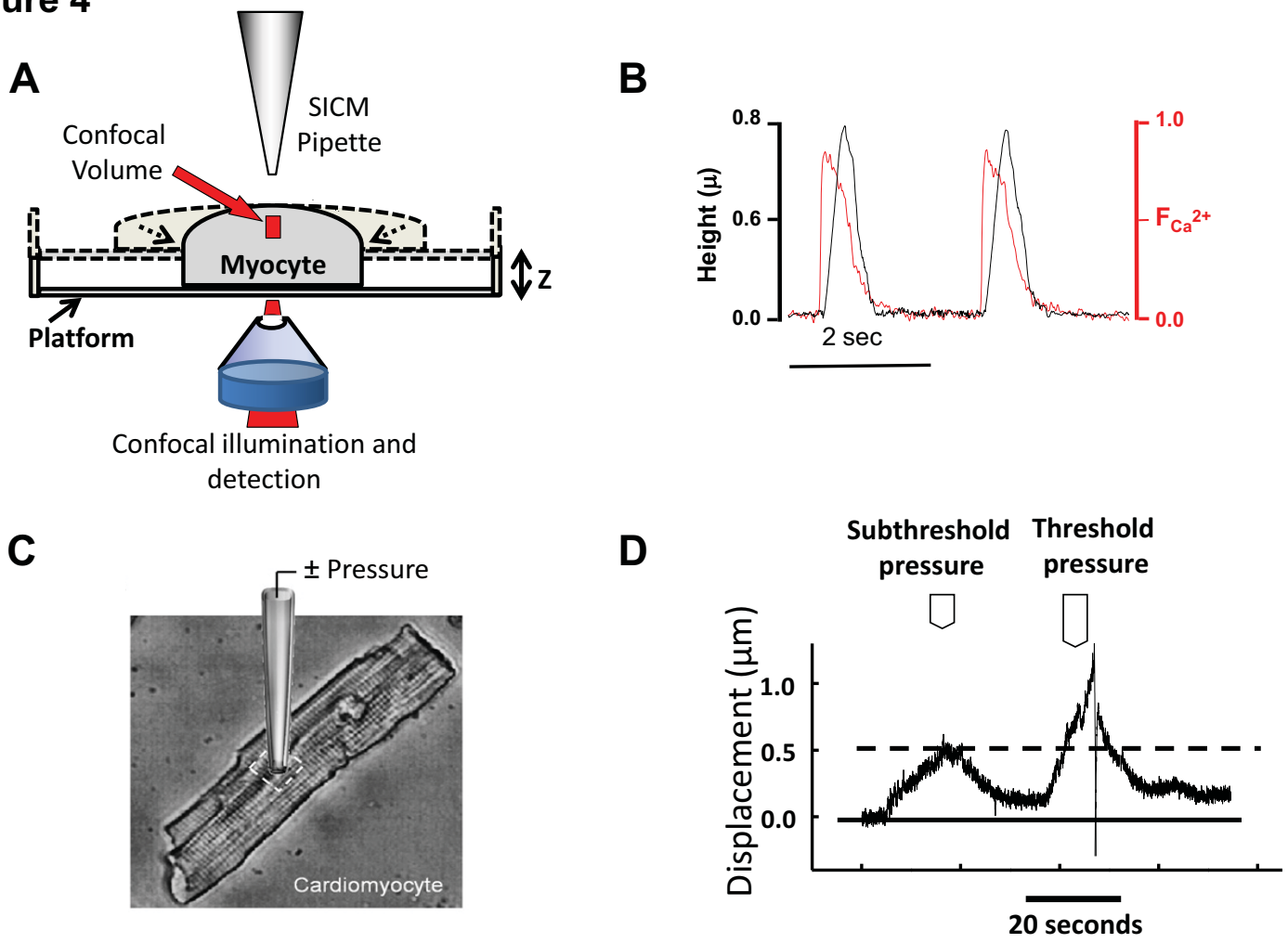
A
SICM
Pipette
Confocal
Volume
Myocyte
Z
Platform
Confocal illumination and
detection
B
0.8
0.6
0.0
Height (μ)
1.0
$F_{Ca^{2+}}$
0.0
2 sec
C
± Pressure
Cardiomyocyte
D
Subthreshold
pressure
Threshold
pressure
Displacement (μm)
1.0
0.5
0.0
20 seconds

Figure 5

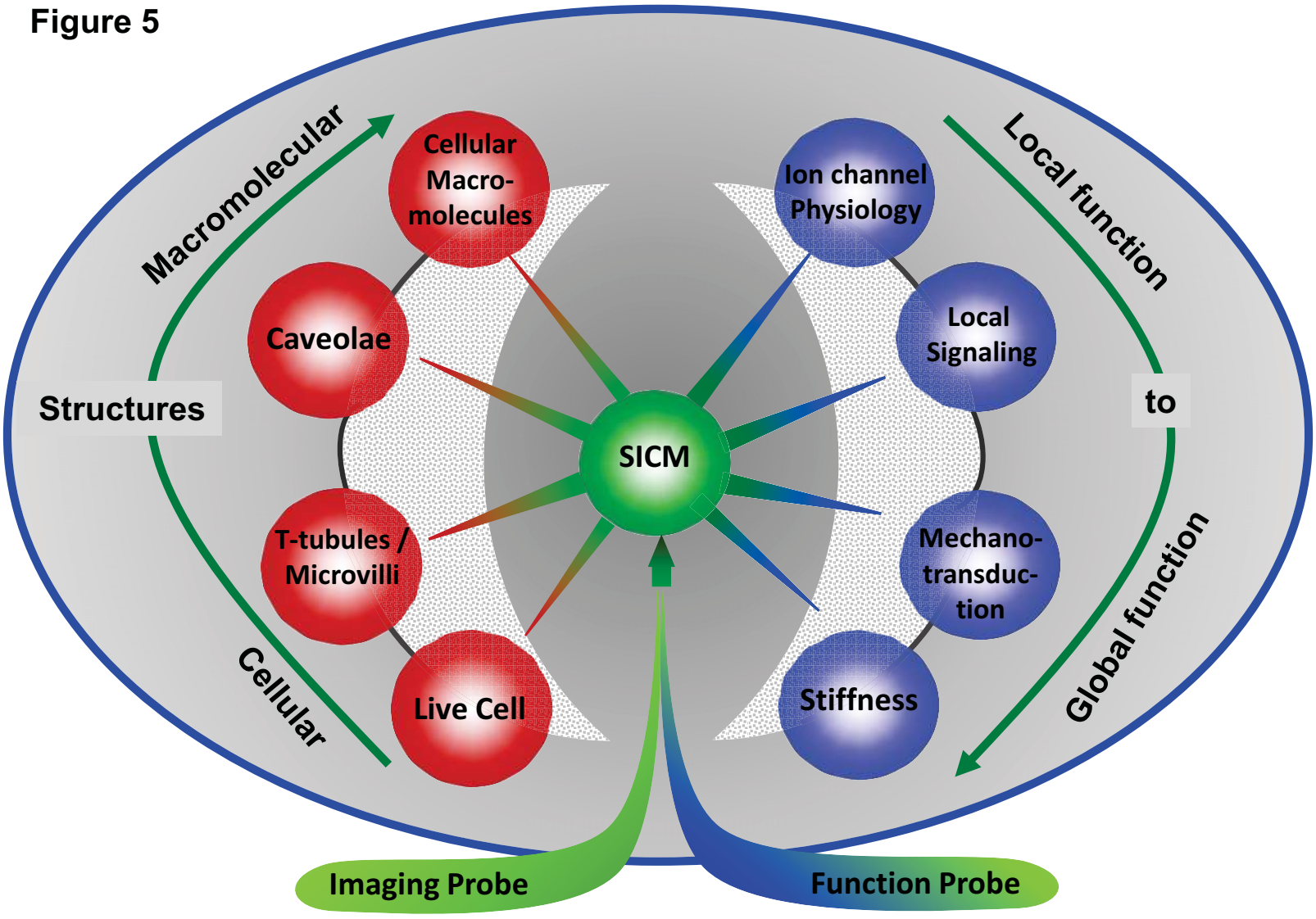
Macromolecular
Structures
Cellular
Local function
to
Global function
Cellular Macro-molecules
Caveolae
T-tubules / Microvilli
Live Cell
SICM
Ion channel Physiology
Local Signaling
Mechano-transduc-tion
Stiffness
Imaging Probe
Function Probe

Table 1

Approx. Resolution (nm)	Microscope System	Principle of Operation	Sample preparation
~200 nm **~5-100 nm**	Optical –Standard (116) Optical - Advanced (101)	Light- wavelength limited* Below light's wavelength*	Stained or unstained in liquid or air
~5– 200 nm	SICM (57, 104, 106)	Ion conductance via nanopipette.	In Ion Conducting Solution
0.5 – 10 nm	Electron - SEM (41, 76) Electron –TEM (18)	Electron beam Impede electrons	Electron conductive sample, vacuum Metal staining, vacuum
~10-50nm	AFM for live cells (81)	Force via sharp probe	In liquid or air